ORIGINAL ARTICLE

Evaluation of ^{99m}Tc-3PRGD$_2$ SPECT imaging on angiogenesis in animal models of lung cancer

Yongkun Wu [ORCID] | Yufei Wang | Zheng Yang | Chuanhui Teng | Zhanlin Guo [ORCID]

Department of Thoracic Surgery, The Affiliated Hospital of Inner Mongolia Medical University, Hohhot, China

Correspondence
Zhanlin Guo, Department of Thoracic Surgery, The Affiliated Hospital of Inner Mongolia Medical University, 1 Tongdaobei Road, Hohhot, Inner Mongolia 010050, China.
Email: nmggzl@163.com

Abstract

Background: The main purpose of the study was to evaluate the activity and selectivity of ^{99m}Tc-3PRGD$_2$ SPECT/CT and ^{18}F-FDG PET-CT in order to detect the neovascularization of A549 cell subcutaneously transplanted tumors, and clarify the relationship among tumor vasculature, hypoxia and cell proliferation in the tumor microenvironment.

Methods: We established a subcutaneous tumor model, and used ^{99m}Tc-3PRGD$_2$ SPECT/CT and ^{18}F-FDG PET-CT when the average tumor size reached 0.3–0.5 cm^3. The mice were anesthetized and sacrificed and the tumors were completely removed for frozen section analysis. We subsequently evaluated the status of neovascularization, hypoxia, as well as cell proliferation via immunofluorescence staining (IF) by detecting CD31, pimonidazole and EdU, respectively.

Results: There was a significant positive correlation ($r = 0.88$, $p < 0.05$) between the microvascular density (41.20 ± 18.60) and tumor to nontumor ratio (T/M), which was based on the value of ^{99m}Tc-3PRGD$_2$ (4.20 ± 1.33); meanwhile, no significance ($r = -0.16$, $p > 0.05$) was found between the T/M and hypoxic area (116.71 ± 9.36). Neovascular proliferation was particularly vigorous in the parenchymal region of the tumor, while the cells around the cavity were generally hypoxic. ^{99m}TC-3PRGD$_2$ SPECT/CT was more specific than ^{18}F-FDG PET-CT in detecting malignant tumors.

Conclusion: Both ^{99m}TC-3PRGD$_2$ and ^{18}F-FDG PET-CT can be used for the detection of malignant tumors, but the specificity and accuracy of ^{99m}TC-3PRGD$_2$ are better. The subcutaneous tumors showed a heterogeneous microenvironment as a result of neovascularization, a high proliferation rate of cancer cells as well as subsequent hypoxia, while most of the hypoxic areas appeared around the cavities of the vessels.

KEYWORDS
^{18}F-FDG PET-CT, ^{99m}Tc-3PRGD$_2$ SPECT, Hypoxia, Proliferation, Tumor Microenvironment

INTRODUCTION

Lung cancer is the most common malignancy with the highest mortality rate worldwide.[1] Metastasis is the major reason for the poor prognosis of lung cancer patients. Tumor vasculature promotes tumor growth and regulates the development of tumor metastasis. Meanwhile, tumor angiogenesis is mediated by the tumor microenvironment (TME). The TME is complex and dynamic, and consists of tumor cells, stromal cells including fibroblasts, endothelial and immune cells as well as extracellular components.[2,3] The TME frequently appears to be highly hypoxic when the tumor diameter is around 2 mm or less with tumors of relatively small volume with a low proliferation rate.[4,5] Once the blood vessels develop, tumor cells receive essential oxygen and nutrients, resulting in rapid cell proliferation. However rapid cell proliferation leads to hypoxia within tumor tissue, which subsequently promotes tumor angiogenesis.[6] Since neovascularization, cell proliferation and hypoxia show close crosstalk in the tumor microenvironment,

exploring the detailed mechanism may provide strong evidence for early diagnosis and a potential strategy for treatment of malignant tumors.

Nuclear medicine techniques have unique advantages in malignancy imaging providing valuable evidence for the diagnosis of malignant tumors. At present, ^{18}F-FDG positron emission tomography-computed tomography (^{18}F-FDG PET-CT) is the most commonly used method for the detection of malignant tumors in clinical studies, although it is less satisfying due to poor specificity, especially when detecting brain and intestinal tumors. Currently, ^{99m}Tc-3PRGD$_2$ single photon emission computed tomography has been clinically applied to diagnose tumors and other diseases.[7,8,9,11] RGD is a peptide sequence consisting of arginine (R)-glycine (G)-aspartate (D), which targets the αvβ3 on neovascular endothelial cells surface. Thus tissues with vigorous neovascularization show a high uptake of RGD. Therefore, radionuclide-labeled RGD can be used to specifically detect tumors with active neovascularization.[10-12]

Pathological tests provide a good assessment of the relationship among vascularization and cellular proliferation as well as hypoxia. Pimonidazole is a nitroimidazole compound which can be taken up by cells. Pimonidazole is excreted via the redox reaction under normal oxygen levels. However, pimonidazole accumulates inside hypoxic cells and may therefore provide a good view to detect tumor hypoxia. Platelet-endothelial cell adhesion molecule (PECAM-1/CD31) is a glycoprotein expressed in vascular endothelial cells, and CD31 is the commonly used marker clarifying the vasculature of the tumor. EdU (5-ethynyl-2-deoxyuridine) as a nucleotide analogue, which is taken up and incorporated into DNA via de novo synthesis in dividing cells, is frequently used to detect highly proliferative cells. Immunofluorescence staining has previously been used[13–15] on solid malignant specimen frozen sections to further elucidate the relationship between tumor vasculature, hypoxia, and cell proliferation.

METHODS

Cell culture

A human lung adenocarcinoma cell line A549 was purchased from Beijing Beina Chuanglian Institute of Biotechnology. A549 cells were maintained in RPMI-1640 supplemented with 10% fetal bovine serum, 1% glutamine, and 1% antibiotic mixture. Cells were cultured under 37°C, 5% CO$_2$ in a thermostatic cell incubator and passaged every 3 days at the ratio according to the manufacturer's recommendations by treatment with 0.25% trypsin for cell detachment.

Mouse model

BALB/c-nu nude mice (4–6-week-old, female, athymic) were purchased from SPF (Beijing) Biotechnology Co. All mouse experiments and procedures were approved by the Administration of Laboratory Animals. The nude mice were housed under specific pathogen-free conditions in Inner Mongolia Medical University, at a constant temperature and humidity. Sterile bedding was changed regularly. Food pellets and water were available ad libitum. Cell suspensions containing 3×10^6 cells (0.2 ml) in PBS were injected using a 1 ml syringe at the top of the upper limb, as shown in Figure 1.

^{99m}Tc-3PRGD$_2$ SPECT/CT and^{18}F-FDG PET-CT

When the average volume of subcutaneous tumors reached 0.3–0.5 cm^3, ^{18}F-FDG PET-CT and ^{99m}Tc-3PRGD$_2$ SPECT/CT imaging was performed. The planar image and tomography were acquired using MG dual probe SPECT/CT and micro-PET-CT in the Affiliated Hospital of Inner Mongolia Medical University. The data were acquired under the guidance of two nuclear medicine physicians, and the region of interest (ROI) was drawn after reconstruction of SPECT and PET-CT data. The ratio Tumor/Muscle of ^{99m}Tc-3PRGD$_2$: The SUM of tumors and muscles was measured (at four random sites) and averaged, separately. Ratio T/M = SUM tumor/SUM muscle. The average uptake value of ^{18}F-FDG (% ID/g) in ROIs were calculated.

Immunohistochemistry

Pimonidazole was administered via tail vein injection 1 h before animal sacrifice (120 μl, 60 mg/kg, diluted in saline). Intact tumors were exfoliated, embedded in OCT, stored at −80°C, and sectioned at a thickness of 3–4 um. Frozen sections were stored at −20°C and immunofluorescence staining was performed on adjacent sections.

Vasculature and hypoxia

Sections were dehydrated at room temperature for 15 min, then fixed with 4% paraformaldehyde for 10 min and incubated with 0.3% Triton X-100 in PBS for permeabilization for 10 min. After washing three times (0.025% triton X-100 in PBS), the tissue section was blocked with 5% BSA in PBS in room temperature for 1 h. The primary antibody was then applied and incubated overnight at 4°C (CD31 rabbit polyclonal antibody, 1:200). The secondary antibody selected was applied on day 2 after washing three times (R-PE-goat anti-rabbit IgG H + L, red,1:100). Sections were then incubated with FITC-conjugated anti-pimonidazole monoclonal antibody (1:50, green), for 2 h at 37°C and the slides were mounted after 10 min incubation with 50 μl of DAPI solution (blue). Images were acquired with fluorescence microscope.

Proliferation and hypoxia

EdU staining was applied to the sections previously described, which were then incubated with Click-it reaction mixture (1:500, 100 μl) labeled with YF594 azide dye (red) for 30 min followed by 10 min of DAPI incubation and slide mounting. Images were acquired with a fluorescence microscope.

FIGURE 1 Procedure for establishing subcutaneous tumor

Image analysis

Microvascular density

Microvascular density was detected and calculated based on the method previously developed by Weidner in 1991. Briefly, we employed immunofluorescence staining to detect the vascular endothelial cell within the tumor tissue. Microvascular density was then determined by counted vascular endothelial cells by MVD = number of vessels (n)/area (cm^2).

Proliferation

The non-necrotic tumor tissue area was selected and imaged under fluorescence microscope after EdU labeling. The number of cells was counted using the trainable Weka segmentation plugin in Fiji software (Image J), by which the EdU positive cells and the total number of cells in the image was acquired. The proliferation rate of the tumor was calculated based on the ratio of EdU positive cell number to the total cell number.

Hypoxia

Pimonidazole accumulates in the cytoplasm of cells, and pimonidazole labeled hypoxic cells are regionally distributed. The mean fluorescence intensity of the hypoxia was calculated according to the formula: fluorescence intensity (mean) = fluorescence intensity of the hypoxia / area of the hypoxia region.[16-18]

TABLE 1 Correlation analysis between ^{99m}Tc-3PRGD$_2$ and vascularity

| Variable	T/M	*p*-value
CD31	0.883*	<0.05
Pimonidazole	−0.159*	>0.05

*$p < 0.05$.

Statistical analysis

All data are expressed as mean ± SEM. Pearson's correlation analysis was performed using SPSS 26.0 statistical software, and $p < 0.05$ was considered statistically significant.

RESULTS

Imaging results of ^{99m}Tc-3PRGD$_2$ and ^{18}F-FDG

The tumor-bearing mice underwent SPECT imaging 2 h after RGD administration, which made it possible to clearly
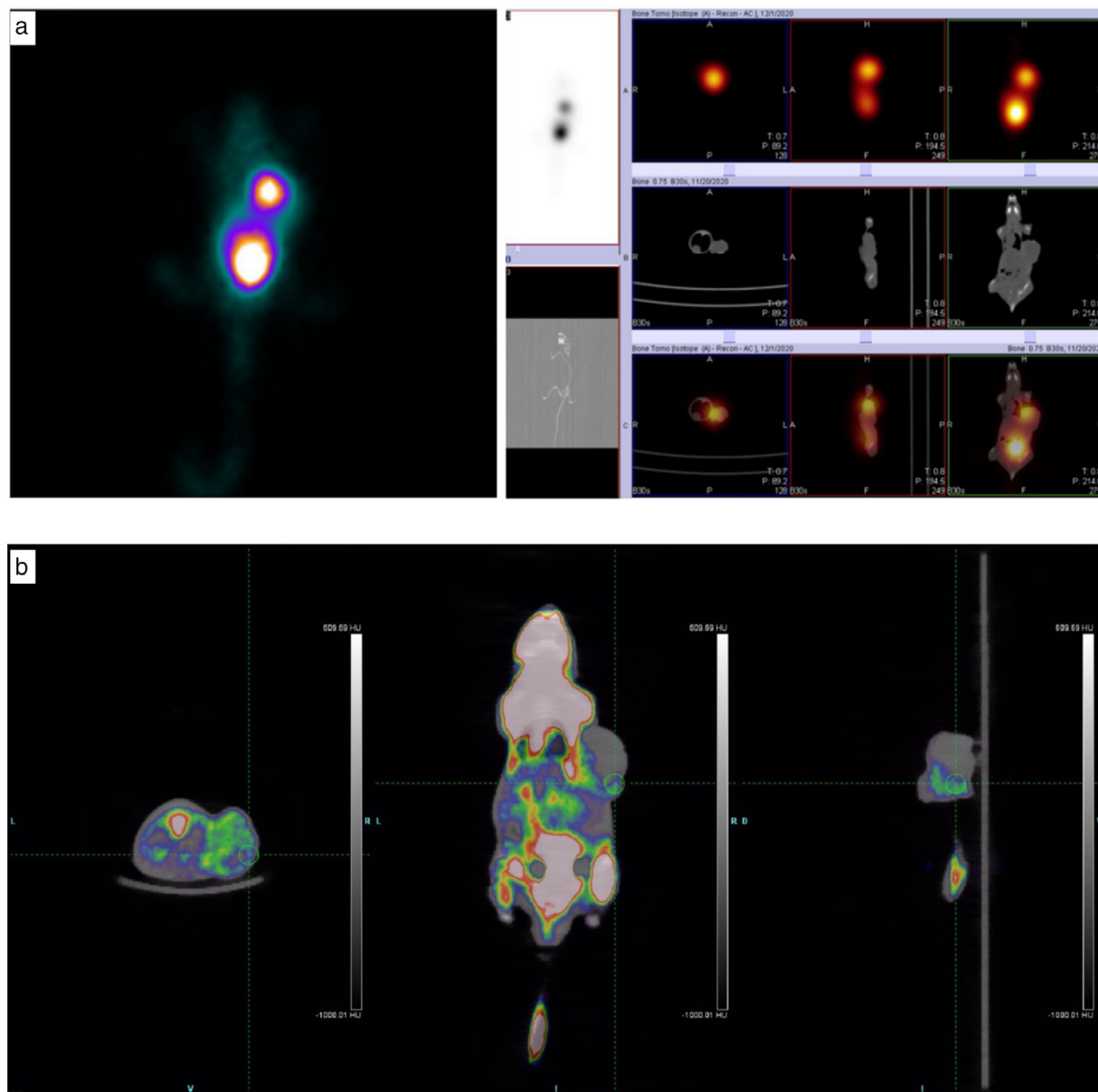
FIGURE 2 (a) ^{99m}Tc-3PRGD$_2$ SPECT/CT image of mouse, radioactive RGD mainly accumulates in the tumor and bladder. (b) ^{18}F-FDG PET-CT image of mouse, lack of specificity with nonuniform distribution of FDG in tumor, which is not distinguishable from other organs

visualize the tumor and bladder. The tumor/muscle (T/ M) ratio was 4.20 ± 1.33. A strong radioactive signal was detected inside the tumor, proving that RGD was prone to accumulate in tumor tissue. There was almost no uptake in other sites such as brain and bone. Highly radioactive signals were also detected in the bladder of mice, which suggested that the ^{99m}Tc-3PRGD$_2$ is mainly metabolized through the urinary system. In Table 1 the T/M value of ^{99m}Tc-3PRGD$_2$ (4.20 ± 1.33) showed a significant positive correlation ($r = 0.88$, $p < 0.05$) with microvascular density (41.20 ± 18.60), which indicated that RGD mainly detecting neovascularization in tumors, can be used to assess the amount of neovascularization and also the efficacy of anti-vascular therapy. There was no significant correlation ($r = -0.16$, $p > 0.05$) between the T/M (4.20 ± 1.33) and

the fluorescence intensity of pimonidazole (116.71 ± 9.36). The tumor-bearing mice underwent PET-CT imaging 1 h after administration of ^{18}F-FDG (working concentration 2.1% ID/g, in tumor). The nonuniform distribution of ^{18}F-FDG in tumors may be related to tumor necrosis. Moreover, other tissue also showed nonspecific signal of ^{18}F-FDG, especially in muscle, brain and the gastrointestinal tract.

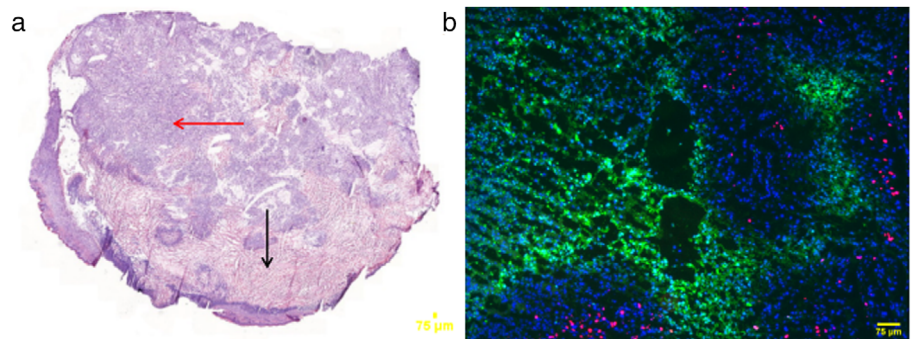## The relationship between vasculature, proliferation and hypoxia

The tumor growth extended in all directions. The neovascularization and cell proliferation at the edge of the tumor were relatively vigorous. However, this may lead to the
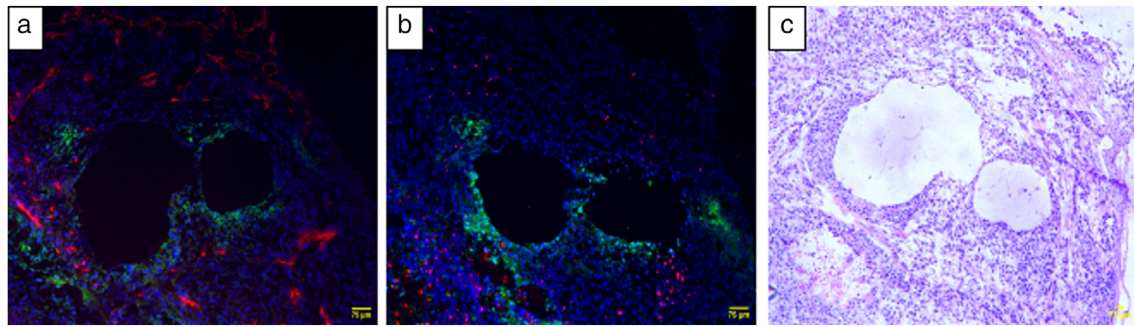
FIGURE 3 (a) Immunofluorescence staining image of CD31 and pimonidazole, CD31(red), pimonidazole (green), nucleus(blue). (b) Immunofluorescence image of EdU and pimonidazole, EdU(red), pimonidazole(green), nucleus(blue). (c) Representative image of H&E staining (×20)

FIGURE 4 (a) Hematoxylin & eosin (H&E) staining of the tumor. The black arrow marks the necrotic area, and the red is the normal tumor nodule part. (b) Immunofluorescence image of tumor tissue labeled by EdU and pimonidazole. (×20)

FIGURE 5 (a) The relationship between blood vessels and hypoxia inside tumor nodules under normoxia. CD31(red), hypoxic (green), nucleus (blue). (b) The relationship between proliferation and hypoxia, EDU (red), hypoxic (green), nucleus (blue) (×20).
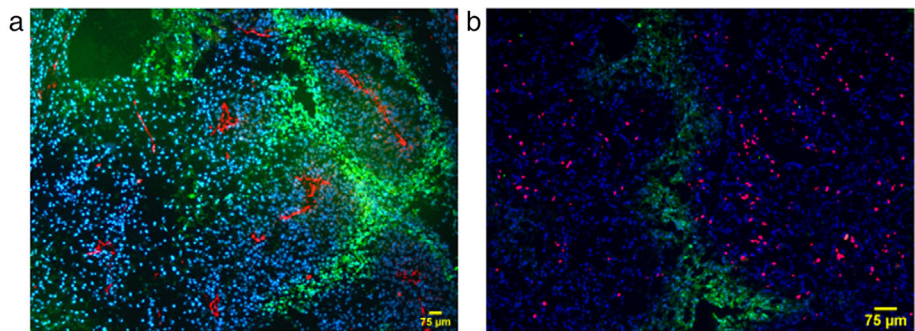
formation of cavities due to rapid growth. As shown in Figure 3, during the growth process, there appeared to be more blood vessels and cavities at the tumor edge area; the cells around those cavities are usually hypoxic. With the tumor growing, the number of cavities will gradually increase, which in turn destroy the blood vessels and lead to hemorrhagic necrosis of the tumor. According to our current results, compared with smaller tumors, when the tumor diameter reached 1 cm, more necrotic areas were visible. As shown by the black arrows in Figure 4a, the tumor cells within these areas were sparse and scattered, without the presence of proliferating cells and lack of blood vessels. Meanwhile the hypoxic cells were also scattered. The cellular structure within these necrotic areas was incomplete because of poor blood supply, and sequentially low proliferative cells contribute to cavities. As shown in Figure 4b, the cavities were surrounded by necrotic and low-proliferative-rate tumor tissue along with lack of obvious blood vessels.

In the normal tumor nodule, the cells are proliferating vigorously with abundant blood vessel formation. As shown in Figure 2a with red arrows, tumor cells are structurally intact and densely organized without obvious cavities or necrosis. In Figure 5, the relationship between neovascularization, proliferation and hypoxia in normal tumor nodules is shown. Neovascularization is relatively vigorous in the marginal parts of the tumor, and hypoxia is mainly in the periphery of the cavities and of the blood vessels. The tumor growth is extended in all directions. The internal structure of the tumor is constantly changing. Proliferation with insufficient blood supply due to excessive growth contributes to necrotic cavities.

DISCUSSION

Various types of RGD peptides have been developed, including some linear and cyclic RGD. Depending on the labeled radionuclide, they may have different methods of detection, in vivo metabolism and other aspects. Cyclic RGD are usually more specific than the linear ones. RGD show high uptake rate in tissues with active neovascularization. In this study, we evaluated the activity and selectivity of ^{99m}Tc-3PRGD$_2$ to detect A549 tumors. The relationships among vascularity, proliferation and tumor hypoxia were also explored.

^{18}F-FDG PET/CT is commonly used to determine the benignity or malignancy of lung masses, utilizing the feature that tumor tissue has active glucose metabolism. However, false positive tests may occur since some benign lesions also exhibit increased glucose metabolism.[19,20] In our study, ^{18}F-FDG showed nonuniform distributions, meanwhile other tissues were also detected with nonspecific uptake of ^{18}F-FDG, especially in muscle. Ever since the advent of RGD, it has been more and more widely used because of its ability to specifically visualize malignant tumors.[21-23] We chose ^{99m}Tc-3PRGD$_2$, a novel RGD dimer, which showed prolonged residence time in the target tissue due to its higher affinity to ligands. In this study, 2 h after injection, the tumor was well defined. Moreover, accumulation of the radiopeptide at the bladder site was also seen, which is consistent with the results of other studies.[24,25] It indicated that RGD can be good image acquisition, and the tumor site shows high uptake of RGD, meanwhile the background of nontarget tissues is low except for the metabolic associated distribution in the bladder. The T/M of this model was 4.20 ± 1.33, which is relatively high compared to previous publications (2.73 ± 0.26).[8] It may be related to the different tumor cell types, since different tumor types have different vascular expression. ^{99m}Tc-3PRGD$_2$ is a reliable radiotracer to identify benign and malignant tumors with good vascular targeting activity. We also found a positive correlation ($r = 0.88$, $p < 0.05$) between the T/M (4.20 ± 1.33) and microvessel density (41.20 ± 18.60) in our experimental model. Therefore, molecular imaging can be a better method to assess the neovascularization of tumors, as a noninvasive technique, showing obvious advantages in the diagnosis, treatment and evaluation of the efficacy of treatment on malignant tumors.

In this experiment, we observed that neovascularization, cell proliferation and hypoxia were widely presented features in the tumor. Proliferation was generally more pronounced in the areas where the neovascularization was vigorous. In contrast, the cells around the cavities were generally hypoxic and had relatively fewer blood vessels. It is therefore assumed that lack of blood supply may lead to cellular hypoxia and necrosis, which in turn promotes the formation of cavities. In advanced solid tumors, necrosis occurs frequently, and along with more hypoxic and relatively fewer viable populations, the cells in necrotic areas presented incomplete cellular structure.

In conclusion, both ^{99m}TC-3PRGD$_2$ and ^{18}F-FDG PET-CT can be used for the detection of malignant tumors, but the specificity and accuracy of ^{99m}TC-3PRGD$_2$ are better. Neovascularization, proliferation and hypoxia were widely present in the subcutaneous tumors, and the areas of hypoxia were more frequent around the vessels and cavities.

CONFLICT OF INTEREST

No author reports any conflicts of interest.

ORCID

Yongkun Wu https://orcid.org/0000-0002-6145-5485
Zhanlin Guo https://orcid.org/0000-0002-7703-5629

REFERENCES

1. Duma N, Santana-Davila R, Molina JR. Non-small cell lung cancer: epid-emiology, screening, diagnosis, and treatment. Mayo Clin Proc. 2019;94:1623–40.
2. Abadjian MZ, Edwards WB, Anderson CJ. Imaging the tumor microenviron-ment. Adv Exp Med Biol. 2017;1036:229–57.
3. Zhou Z, Lu ZR. Molecular imaging of the tumor microenvironment. Adv D-rug Deliv Rev. 2017;113:24–48.
4. Vaupel P, Multhoff G. Fatal alliance of hypoxia-/HIF-1α-driven microenvir-onmental traits promoting cancer progression. Adv Exp Med Biol. 2020;1232:169–76.
5. Li XF, Carlin S, Urano M. Visualization of hypoxia in microscopic tumors by immunofluorescent microscopy. Cancer Res. 2007;67:7646–53.
6. Du Y, Ge Y, Xu Z. Hypoxia-inducible factor 1 alpha (HIF-1α)/vascular en-dothelial growth factor (VEGF) pathway participates in angiogenesis of my ocardial infarction in muscone-treated mice: preliminary study. Med Sci M-onit. 2018;24:8870–7.
7. Ramezanizadeh M, Masterifarahani A, Sadeghzadeh N. 99mTc-D (RGD): mol-ecular imaging probe for diagnosis of αvβ3-positive tumors. Nucl Med Comun. 2020;41:104–9.
8. Zhao ZQ, Yang Y, Fang W. Comparison of biological properties of 99mTc-l-abeled cyclic RGD Peptide trimer and dimer useful as SPECT radiotracers for tumor imaging. Nucl Med Biol. 2016;43:661–9.
9. Provost C, Prignon A, Rozenblum-Beddok L. Comparison and evaluation of two RGD peptides labelled with 68Ga or 18F for PET imaging of angiogene is in animal models of human glioblastoma or lung carcinoma. Oncotarget. 2018;9:19307–16.
10. Dal Corso A, Pignataro L, Belvisi L. αvβ3 integrin-targeted peptide/-peptido-mimetic-drug conjugates: In-depth analysis of the linker technology. Curr-Top Med Chem. 2016;16:314–29.
11. Dong X, Yu Y, Wang Q. Interaction mechanism and clustering among RGDPeptides and integrins. Mol Inform. 2017;36:5–6.
12. Yu YP, Wang Q, Liu YC. Molecular basis for the targeted binding of RGD-containing peptide to integrin αVβ3. Biomaterials. 2014;35:1667–75.
13. Chen X, Maniotis AJ, Majumdar D. Uveal melanoma cell staining for CD34and assessment of tumor vascularity. Invest Ophthalmol Vis Sci. 2002;43:2533–9.
14. Im K, Mareninov S, Diaz MFP. An introduction to performing immunofluor-escence staining. Methods Mol Biol. 1897;2019:299–311.

15. Adam K, Hunter T. Subcellular localization of histidine phosphory-lated pro-teins through indirect immunofluorescence. Methods Mol Biol. 2020;2077:209–24.

16. Adler J, Parmryd I. Colocalization analysis in fluorescence micros-copy. Met-hods Mol Biol. 2013;931:97–109.

17. Bolte S, Cordelières FP. A guided tour into subcellular colocalization analysi-sin light microscopy. J Microsc. 2006;224:213–32.

18. Dunn KW, Kamocka MM, McDonald JH. A practical guide to evalu-ating co-localization in biological microscopy. Am J Physiol Cell Phy-siol. 2011;300:C 723–42.

19. Durante S, Dunet V, Gorostidi F. Head and neck tumors angiogenesis imagi-ng with 68Ga-NODAGA-RGD in comparison to 18F-FDG PET/CT: a pilot st-udy. EJNMMI Res. 2020;10:47.

20. Wang T, Wang Z. Application of metabolic parameters measured by 18F-F-DG PET/CT in the evaluation of the prognosis of non-small cell lung ca-ncer. Zhongguo Fei Ai Za Zhi. 2019;22:167–72.

21. Xu D, Zhao ZQ, Chen ST, Yang Y, Fang W, Liu S. Iminodiacetic acid as bifunctional linker for dimerization of cyclic RGD peptides. Nucl Med Biol. 2017;48:1–8.

22. Sun CC, Qu XJ, Gao ZH. Integrins: players in cancer progression and targets in cancer therapy. Anticancer Drugs. 2014;25:1107–21.

23. Paweletz N, Knierim M. Tumor-related angiogenesis. Crit Rev Oncol Hematol. 1989;9:197–242.

24. Huang C, Zheng Q, Miao W. Study of novel molecular probe 99mTc-3PRGD2 in the diagnosis of rheumatoid arthritis. Nucl Med Com-mun. 2015;36:1208–14.

25. Jin X, Meng Y, Zhu Z. Elevated 99mTc 3PRGD2 activity in benign metastasizing leiomyoma. Clin Nucl Med. 2013;38:117–9.